International Journal of Solids and Structures 46 (2009) 1413–1422

Contents lists available at ScienceDirect

International Journal of Solids and Structures

journal homepage: www.elsevier.com/locate/ijsolstr

Effect of interface stresses on the image force and stability of an edge dislocation inside a nanoscale cylindrical inclusion

Q.H. Fang [a,*], Y.W. Liu [a], B. Jin [a], P.H. Wen [b]

[a] College of Mechanics and Aerospace, Hunan University, Changsha 410082, PR China
[b] School of Engineering and Material Sciences, Queen Mary, University of London, London E1 4NS, UK

ARTICLE INFO

Article history:
Received 12 August 2008
Received in revised form 22 October 2008
Available online 3 December 2008

Keywords:
Edge dislocation
Interface stress
Image force
Nanoscale inclusion
Dislocation stability

ABSTRACT

Dislocation mobility and stability in inclusions can affect the mechanical behaviors of the composites. In this paper, the problem of an edge dislocation located within a nanoscale cylindrical inclusion incorporating interface stress is first considered. The explicit expression for the image force acting on the edge dislocation is obtained by means of a complex variable method. The influence of the interface effects and the size of the inclusion on the image force is evaluated. The results indicate that the impact of interface stress on the image force and the equilibrium positions of the edge dislocation inside the inclusion becomes remarkable when the radius of the inclusion is reduced to nanometer scale. The force acting on the edge dislocation produced by the interface stress will increase with the decrease of the radius of the inclusion and depends on the inclusion size which differs from the classical solution. The stability of the dislocation inside a nanoscale inclusion is also analyzed. The condition of the dislocation stability and the critical radius of the inclusion are revised for considering interface stresses.

1. Introduction

Many physical properties of solids, such as plasticity, strength, and some optical and magnetic characteristics are structure-sensitive. The crystal lattice imperfections (dislocations, disclinations, pores, etc.) can drastically change the physical characteristics of materials (Gryaznov and Trusov, 1993). Therefore, the interaction of inclusions with dislocations of different kinds is of considerable importance for understanding the physical behavior of crystalline solids. For example, it can provide important information concerning certain strengthening and hardening mechanism in a number of materials (Nembach, 1996). Due to its importance, a number of contributions have been conducted on this topic during the last several decades (Dundurs and Mura, 1964; Hirth and Lothe, 1982; Luo and Chen, 1991; Stagni, 1993; Zhang and Qian, 1996; Xiao and Chen, 2001; Liu et al., 2004; Ma and Lu, 2006; Wang and Sudak, 2006; Wang et al., 2007; Takahashi and Ghoniem, 2008).

The mobility and stability of dislocations inside dispersed particles or second phase inclusions can also significantly affect the physical behaviors of alloys and composites (Nembach, 1996). On the other hand, the image stress of the dislocation inside an elastic cylinder may be important for dislocation dynamics simulations of the plastic deformation of a cylinder (Weinberger and Cai, 2007). Some solutions for the problem of the dislocation inside the inclusion in composites have been obtained and used to discuss the mobility and the equilibrium points of the dislocation (Dundurs and Sendeckyj, 1965; Warren, 1983; Qaissaunee and Santare, 1995; Stagni, 1999). These studies did not investigate the stability of the dislocation inside the inclusion and were restricted to the case that the size of the inclusion equals to the micron dimension or larger than it. In general, when the dimensions of solids are comparable with the correlation length of physical phenomena (e.g., the Cooper-pair length, an exciton size, a dislocation pileup length, etc.), a detailed revision of all physical properties of solids becomes necessary, usually referred to as size effects (Gryaznov et al., 1991). When the size of the inclusion (second phase) is very small (of the order of nanometers), an influence of size effects of the nanoscale inclusion on the behavior of lattice defects in the inclusion ought to drastically change the physicomechanical characteristic of the composites. Theoretical results concerning the behavior of dislocations in small particles and nanocrystals have been reported (Gryaznov et al., 1989, 1991; Gryaznov and Trusov, 1993; Romanov, 1995), where the problem of stability of dislocations in nanovolumes has been considered and the existence of the critical size of dislocation stability in nanoparticles or nanograins has been predicted. Below this size which depends on such material parameters as elastic modulus and lattice resistance to the dislocation motion, the dislocations are unstable in the nanovolume interior. Some other studies on the dislocation stability had also been considered (Schoeck, 1997; Wang, 1998; Yoo et al., 1999; Chen and Biner, 2005).

* Corresponding author. Tel.: +86 731 8823517; fax: +86 731 8822330.
E-mail address: fangqh1327@tom.com (Q.H. Fang).

0020-7683/$ - see front matter © 2008 Elsevier Ltd. All rights reserved.
doi:10.1016/j.ijsolstr.2008.11.013

The interface condition is an important factor for studying dislocation mobility and stability inside inclusions. When the size of the inclusion is of the order of nanometer, the inclusion–matrix interface energy cannot be neglected because of the increased contribution to the total energy from the interface (Duan et al., 2005). A generic and mathematical exposition for elastic isotropic solids with the surface/interface energy (surface/interface stress) has been presented by Gurtin and his co-workers (Gurtin and Murdoch, 1975; Gurtin et al., 1998). Utilizing this interface model (This model is the so-called interface stress model), great effort has been made recently to understand some unusual phenomena related to the interface stress in nanocomposites (Sharma et al., 2003; Sharma and Ganti, 2004; Lim et al., 2006; Chen and Dvorak, 2006; Duan and Karihaloo, 2007; Quang and He, 2007; Chen et al., 2007; Tian and Rajapakse, 2007). These studies indicate that the interface effects is a critical factor in the physical behavior of the materials containing inclusions of a sufficiently small size.

Recently, the interaction between an edge dislocation and a circular inclusion with interface stress has been considered by Fang and Liu (2006). In their paper, an edge dislocation is assumed to be located inside the infinite matrix and the image force acting on the dislocation is given. In the present work, the problem of an edge dislocation located within a nanoscale inclusion is first investigated by using the surface/interface stress model which proposed by Gurtin and Murdoch (1975). The effect of the interface stress on the mobility and equilibrium positions of the edge dislocation in the inclusion is evaluated. In addition, the stability of edge dislocations inside a nanoscale inclusion is also studied.

2. Statement of the problem

The basic model to be treated is that of an infinite elastic medium with the elastic properties κ_2 and μ_2 containing a circular nanoscale inclusion of a radius R with the elastic properties κ_1 and μ_1, where μ_j $(j=1,2)$ is the shear modulus and $\kappa_j = 3-4\upsilon_j$ for plane strain state (υ_j is the Poisson's ratio). An edge dislocation with Burgers vector (b_x, b_y) is assumed to be located inside the circular inclusion at the point z_0 as shown in Fig. 1.

Following the work of Gurtin and Murdoch (1975), the elastic field within the bulk solid is described by the differential equations of classical elasticity, while the interface has its own elastic constants and is characterized by an additional constitutive law. Under the assumption that the interface region adheres to the bulk solid without slipping and the body forces are vanishes, the equilibrium and constitutive equations for isotropic case have been given in Sharma et al. (2003). For the current problem, the boundary conditions at the interface can be obtained from the generalized Young–Laplace equations.

$$u_{x1}^{+}(t)-u_{x2}^{-}(t)=0 \qquad u_{y1}^{+}(t)-u_{y2}^{-}(t)=0 \quad |t|=R \tag{1}$$

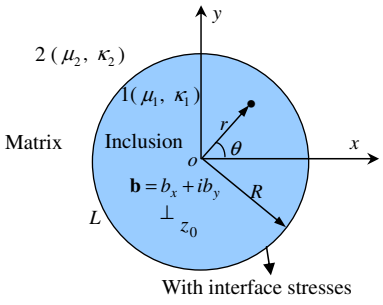

Fig. 1. Schematic diagram of an edge dislocation inside a nanoscale cylindrical inclusion.

$$\sigma_{rr1}^{+}(t)-\sigma_{rr2}^{-}(t)=-\frac{\sigma_{\theta\theta}^{0}(t)}{R} \qquad \sigma_{r\theta1}^{+}(t)-\sigma_{r\theta2}^{-}(t)=\frac{1}{R}\frac{\partial\sigma_{\theta\theta}^{0}(t)}{\partial\theta} \quad |t|=R \tag{2}$$

where u_x and u_y are displacement components in the Cartesian coordinates, σ_{rr} and $\sigma_{r\theta}$ are stress components in polar coordinates system r and θ, the superscripts + and − denote the boundary values of a physical quantity when z approaches the interface from the inclusion and the matrix, respectively, the subscripts 1 and 2 represent the inclusion and the matrix regions, the superscript "0" denotes the circular interface. In addition, the constitutive equation for the interface region is given as (Duan et al., 2005)

$$\sigma_{\theta\theta}^{0}(t)=(2\mu^{0}+\lambda^{0})\varepsilon_{\theta\theta}^{0}(t) \tag{3}$$

where $\sigma_{\theta\theta}^{0}$ and $\varepsilon_{\theta\theta}^{0}$ denote interfacial stress and strain, μ^0 and λ^0 are interfacial Lame constants. For a coherent interface, the interfacial strain $\varepsilon_{\theta\theta}^{0}$ is equal to the associated tangential strain in the abutting bulk materials. With semi-coherent or incoherent interfaces, an additional measure of the interfacial strain is required. In the following, we will study the case for a coherent interface.

Considering the additional constitutive equation for interface region in Eq. (3) and the constitutive equation for the bulk solid, the stress discontinuity conditions in Eq. (2) at the interface can be rewritten as

$$\sigma_{rr1}^{+}(t)-\sigma_{rr2}^{-}(t)=-\frac{2\mu^{0}+\lambda^{0}}{4R\mu_1(\lambda_1+\mu_1)}[(\lambda_1+2\mu_1)\sigma_{\theta\theta1}(t)-\lambda_1\sigma_{rr1}(t)] \tag{4}$$

$$\sigma_{r\theta1}^{+}(t)-\sigma_{r\theta2}^{-}(t)=\frac{2\mu^{0}+\lambda^{0}}{4R\mu_1(\lambda_1+\mu_1)}\left[(\lambda_1+2\mu_1)\frac{\partial\sigma_{\theta\theta1}(t)}{\partial\theta}-\lambda_1\frac{\partial\sigma_{rr1}(t)}{\partial\theta}\right] \tag{5}$$

where μ_1 and λ_1 are Lame constants of the inclusion.

3. General solution of basic model

The stress and displacement components in the bulk solid can be expressed in terms of two Muskhelishvili's complex potentials $\Phi(z)$ and $\Psi(z)$ (Muskhelishvili, 1975). For the problem under consideration, the complex potentials $\Phi_1(z)$ and $\Psi_1(z)$ in the inclusion region can be taken in the following forms (Qaissaunee and Santare, 1995):

$$\Phi_1(z)=\frac{\gamma_1}{z-z_0}+\Phi_{10}(z) \quad |z|<R \tag{6}$$

$$\Psi_1(z)=\frac{\overline{\gamma_1}}{z-z_0}+\frac{\gamma_1\bar{z}_0}{(z-z_0)^2}+\Psi_{10}(z) \quad |z|<R \tag{7}$$

where $\gamma_1=\frac{\mu_1}{\pi(1+\kappa_1)}(b_y-ib_x)$, $\Phi_{10}(z)$ and $\Psi_{10}(z)$ are unknown and analytical complex functions in the inclusion region.

The complex potentials outside the inclusion are holomorphic and can be taken in the following forms for a large value of $|z|$.

$$\Phi_2(z)=\frac{\gamma_2}{z}+O\left(\frac{1}{z^2}\right), \quad \Psi_2(z)=\frac{\overline{\gamma_2}}{z}+O\left(\frac{1}{z^2}\right) \tag{8}$$

where $\gamma_2=\frac{\mu_2}{\pi(1+\kappa_2)}(b_y-ib_x)$.

To treat the boundary conditions on the interface, it is convenient to introduce the following analytic functions:

$$\Omega_1(z)=-\overline{\Phi_1}\left(\frac{R^2}{z}\right)+\frac{R^2}{z}\overline{\Phi_1'}\left(\frac{R^2}{z}\right)+\frac{R^2}{z^2}\overline{\Psi_1}\left(\frac{R^2}{z}\right) \quad |z|>R \tag{9}$$

$$\Omega_2(z)=-\overline{\Phi_2}\left(\frac{R^2}{z}\right)+\frac{R^2}{z}\overline{\Phi_2'}\left(\frac{R^2}{z}\right)+\frac{R^2}{z^2}\overline{\Psi_2}\left(\frac{R^2}{z}\right) \quad |z|<R \tag{10}$$

Considering Eqs. (6)–(8), Eqs. (9) and (10) have the following forms:

$$\Omega_1(z)=-\frac{\gamma_1}{z-z^*}+\frac{\overline{\gamma_1}z^*(z_0-z^*)}{\bar{z}_0(z-z^*)^2}+\Omega_{10}(z) \quad |z|>R \tag{11}$$

$$\Omega_2(z)=\frac{\gamma_2}{z}+\Omega_{20}(z) \quad |z|<R \tag{12}$$

where $z^* = R^2/\overline{z_0}$. $\Omega_{10}(z)$ and $\Omega_{20}(z)$ are holomorphic complex functions.

With the aid of Eqs. (9) and (10), the displacement continuity conditions on the entire circular interface in Eq. (1) can be expressed as

$$\left[\frac{\kappa_1}{\mu_1}\Phi_1(t) - \frac{1}{\mu_2}\Omega_2(t)\right]^+ = \left[\frac{\kappa_2}{\mu_2}\Phi_2(t) - \frac{1}{\mu_1}\Omega_1(t)\right]^- \quad |t| = R \tag{13}$$

According to the generalized Liouville theorem (Muskhelishvili, 1975) and Eqs. (6)–(12), Eq. (13) leads to

$$h(z) = \begin{cases} \Phi_1(z)(\kappa_1/\mu_1) - \Omega_2(z)/\mu_2 & |z| < R \\ \Phi_2(z)(\kappa_2/\mu_2) - \Omega_1(z)/\mu_1 & |z| > R \end{cases} \tag{14}$$

where $h(z) = \frac{\kappa_1}{\mu_1}\frac{\gamma_1}{z-z_0} + \frac{1}{\mu_1}\left[\frac{\gamma_1}{z-z^*} - \frac{\overline{\gamma_1}z^*(z_0-z^*)}{\bar{z}_0(z-z^*)^2}\right] - \frac{1}{\mu_2}\frac{\gamma_2}{z} + D_1$. With the help of Eq. (9) and the second equation in Eq. (14), the unknown constant D_1 can be obtained

$$D_1 = \overline{\Phi_1(0)}/\mu_1 \tag{15}$$

The stress boundary conditions Eqs. (4) and (5) can be expressed as

$$\begin{aligned} &\left[\Phi_1(t) + \Omega_2(t) + (a+b)\Phi_1(t) + (a+b)t\Phi_1'(t) + a\overline{\Omega_1}(R^2/t) - a(R^2/t)\overline{\Omega_1'}(R^2/t)\right]^+ \\ &= \left[\Phi_2(t) + \Omega_1(t) - a\Omega_1(t) - at\Omega_1'(t) - (a+b)\overline{\Phi_1}(R^2/t)\right. \\ &\quad \left.+(a+b)(R^2/t)\overline{\Phi_1'}(R^2/t)\right]^- \quad |t| = R \end{aligned} \tag{16}$$

where $a = \frac{2\mu^0+\lambda^0}{4R\mu_1}$ and $b = \frac{2\mu_1(2\mu^0+\lambda^0)}{4R\mu_1(\lambda_1+\mu_1)}$.

Similarly, by using the generalized Liouville theorem, it leads to

$$g(z) = \begin{cases} \Phi_1(z) + \Omega_2(z) + (a+b)\Phi_1(z) + (a+b)z\Phi_1'(z) + a\overline{\Omega_1}(R^2/z) \\ \quad -a(R^2/z)\overline{\Omega_1'}(R^2/z) & |z| < R \\ \Phi_2(z) + \Omega_1(z) - a\Omega_1(z) - az\Omega_1'(z) - (a+b)\overline{\Phi_1}(R^2/z) \\ \quad +(a+b)(R^2/z)\overline{\Phi_1'}(R^2/z) & |z| > R \end{cases} \tag{17}$$

where

$$\begin{aligned} g(z) = {} & (a+b-1)\frac{\gamma_1}{z-z_0} - (a+b)\frac{z\gamma_1}{(z-z_0)^2} + \frac{\gamma_2}{z} \\ & + (1-a)\left[-\frac{\gamma_1}{z-z^*} + \frac{\overline{\gamma_1}z^*(z_0-z^*)}{\bar{z}_0(z-z^*)^2}\right] \\ & + a\left[\frac{\overline{\gamma_1}zz_0}{R^2(z-z_0)} - \frac{\overline{\gamma_1}zz_0^2}{R^2(z-z_0)^2} + \frac{\gamma_1\overline{z^*}(\overline{z_0}-\overline{z^*})z^2z_0}{R^4(z-z_0)^2}\right. \\ & \left. - \frac{2\gamma_1\overline{z^*}(\overline{z_0}-\overline{z^*})z^2z_0^2}{R^4(z-z_0)^3}\right] - a\left[\frac{\gamma_1 z}{(z-z^*)^2} - \frac{2\overline{\gamma_1}z^*(z_0-z^*)z}{\bar{z}_0(z-z^*)^3}\right] \\ & -(a+b)\frac{\overline{\gamma_1}z}{\overline{z_0}}\left[\frac{z^*}{(z-z^*)^2} - \frac{1}{z-z^*}\right] + D_2 \end{aligned} \tag{18}$$

The unknown constant D_2 in Eq. (18) can be determined by Eq. (9) and the second equation in Eq. (18) as $z \to \infty$.

$$D_2 = -(1+b)\overline{\Phi_1(0)} - a\left[\frac{\overline{\gamma_1}z_0}{R^2} + \frac{\gamma_1\overline{z^*}(\overline{z_0}-\overline{z^*})z_0}{R^4}\right] - (a+b)\frac{\overline{\gamma_1}}{\overline{z_0}} \tag{19}$$

From Eqs. (14) and (18), we have

$$\begin{aligned} &\left(\frac{\mu_2\kappa_1}{\mu_1} + 1 + a + b\right)\Phi_1(z) + (a+b)z\Phi_1'(z) + a\overline{\Omega_1}\left(\frac{R^2}{z}\right) \\ &- a\frac{R^2}{z}\overline{\Omega_1'}\left(\frac{R^2}{z}\right) = g(z) + \mu_2 h(z) \end{aligned} \tag{20}$$

$$\begin{aligned} &\left(1 - a - \frac{\mu_2}{\mu_1\kappa_2}\right)\Omega_1(z) - az\Omega_1'(z) - (a+b)\overline{\Phi_1}\left(\frac{R^2}{z}\right) \\ &+ (a+b)\frac{R^2}{z}\overline{\Phi_1'}\left(\frac{R^2}{z}\right) = g(z) - \frac{\mu_2}{\kappa_2}h(z) \end{aligned} \tag{21}$$

The substitution of Eqs. (6) and (11) into Eqs. (20) and (21) yields

$$\begin{aligned} &\left(\frac{\mu_2\kappa_1}{\mu_1} + 1 + a + b\right)\Phi_{10}(z) + (a+b)z\Phi_{10}'(z) + a\overline{\Omega_{10}}\left(\frac{R^2}{z}\right) \\ &- a\frac{R^2}{z}\overline{\Omega_{10}'}\left(\frac{R^2}{z}\right) = f_1(z) \end{aligned} \tag{22}$$

$$\begin{aligned} &\left(1 - a - \frac{\mu_2}{\mu_1\kappa_2}\right)\Omega_{10}(z) - az\Omega_{10}'(z) - (a+b)\overline{\Phi_{10}}\left(\frac{R^2}{z}\right) \\ &+ (a+b)\frac{R^2}{z}\overline{\Phi_{10}'}\left(\frac{R^2}{z}\right) = f_2(z) \end{aligned} \tag{23}$$

with

$$\begin{aligned} f_1(z) = {} & (1 - a - \frac{\mu_2}{\mu_1})\left[-\frac{\gamma_1}{z-z^*} + \frac{\overline{\gamma_1}z^*(z_0-z^*)}{\bar{z}_0(z-z^*)^2}\right] \\ & - a\left[\frac{\gamma_1 z}{(z-z^*)^2} - \frac{2\overline{\gamma_1}z^*(z_0-z^*)z}{\bar{z}_0(z-z^*)^3}\right] \\ & - (a+b)\frac{\bar{\gamma}z}{\overline{z_0}}\left[\frac{z^*}{(z-z^*)^2} - \frac{1}{z-z^*}\right] + \mu_2 D_1 + D_2 \end{aligned}$$

and

$$\begin{aligned} f_2(z) = {} & (a+b+1-\frac{\mu_2\kappa_1}{\mu_1\kappa_2})\frac{\gamma_1}{z-z_0} - (a+b)\frac{z\gamma_1}{(z-z_0)^2} + \left(1+\frac{1}{\kappa_2}\right)\frac{\gamma_2}{z} \\ & + a\left[\frac{\overline{\gamma_1}zz_0}{R^2(z-z_0)} - \frac{\overline{\gamma_1}zz_0^2}{R^2(z-z_0)^2} + \frac{\gamma_1\overline{z^*}(\overline{z_0}-\overline{z^*})z^2z_0}{R^4(z-z_0)^2}\right. \\ & \left. - \frac{2\gamma_1\overline{z^*}(\overline{z_0}-\overline{z^*})z^2z_0^2}{R^4(z-z_0)^3}\right] - \frac{\mu_2}{\kappa_2}D_1 - D_2. \end{aligned}$$

The two first order differential equations above can be solved by a power-series method (Muskhelishvili, 1975). Note that the complex potential $\Phi_{10}(z)$ and $\Omega_{10}(z)$ can be taken in the following series expansions:

$$\Phi_{10}(z) = c_0 + \sum_{k=1}^{+\infty} c_k z^k \quad |z| < R \tag{24}$$

$$\Omega_{10}(z) = d_0 + \sum_{k=1}^{+\infty} d_{-k} z^{-k} \quad |z| > R \tag{25}$$

From Eqs. (22)–(25) the unknown coefficients in right-hand side of Eqs. (24) and (25) can be obtained

$$c_0 = \frac{m + e\bar{m}}{1-e^2} \quad d_0 = \frac{\overline{\gamma_1}}{\overline{z_0}} - \frac{\bar{m} + em}{1-e^2} \tag{26}$$

$$\begin{aligned} c_k = {} & \frac{e_2}{e_1}\left[\gamma_1(z^*)^{-k-1} + \frac{\overline{\gamma_1}(z_0-z^*)(k+1)(z^*)^{-k-1}}{\bar{z}_0}\right] - \frac{e_3}{e_1}\frac{\overline{\gamma_1}}{\overline{z_0}}(z^*)^{-k} \\ & - \frac{e_4}{e_1}\frac{\gamma_2}{R^2}\delta_{1k} \quad k \geqslant 1 \end{aligned} \tag{27}$$

$$\begin{aligned} d_{-k} = {} & \frac{e_6}{e_5}\left[\frac{\overline{\gamma_1}(z_0)^{k+1}}{R^2} + \frac{\gamma_1\overline{z^*}(\overline{z_0}-\overline{z^*})(k+1)(z_0)^{k+1}}{R^4}\right] + \frac{e_7}{e_5}\gamma_1(z_0)^{k-1} \\ & + \frac{1}{e_5}\left(1+\frac{1}{\kappa_2}\right)\gamma_2\delta_{1k} \quad k \geqslant 1 \end{aligned} \tag{28}$$

where

$$e=\frac{\mu_2/\mu_1-1-b}{1+b+(\mu_2\kappa_1)/\mu_1},$$

$$e_1=\frac{a(a+b)(1+k)(1-k)}{1+a(k-1)+\mu_2/(\mu_1\kappa_2)}+1+(a+b)(k+1)+(\mu_2\kappa_1)/\mu_1,$$

$$m=\frac{1-a-\mu_2/\mu_1}{\mu_2/\mu_1-1-b}\left[\frac{\gamma_1}{z^*}+\frac{\overline{\gamma_1}(z_0-z^*)}{z^*\overline{z}_0}\right]-\frac{\mu_2/\mu_1-1-2b-a}{\mu_2/\mu_1-1-b}\frac{\gamma_1}{\overline{z}_0}$$
$$-\frac{a}{\mu_2/\mu_1-1-b}\left[\frac{\overline{\gamma_1}z_0}{R^2}+\frac{\gamma_1\overline{z^*}(\overline{z}_0-\overline{z^*})z_0}{R^4}+\frac{\gamma_1}{z_0}\right],$$

$$e_2=1-a(k+1)+\mu_2/\mu_1-\frac{a^2(1+k)(1-k)}{1+a(k-1)+\mu_2/(\mu_1\kappa_2)},$$

$$e_3=(a+b)(k+1)+\frac{a(1+k)[1+(a+b)(k+1)+(\mu_2\kappa_1)/\mu_1]}{1+a(k-1)+\mu_2/(\mu_1\kappa_2)},$$

$$e_4=\frac{a(1+k)}{1+a(k-1)+\mu_2/(\mu_1\kappa_2)}\left(1+\frac{1}{\kappa_2}\right),$$

$$e_5=1+a(k-1)+\mu_2/(\mu_1\kappa_2)+\frac{a(a+b)(1+k)(1-k)}{1+(a+b)(k+1)+(\mu_2\kappa_1)/\mu_1},$$

$$e_6=a(k-1)+\frac{[1-a(k+1)+\mu_2/\mu_1](a+b)(1-k)}{1+(a+b)(k+1)+(\mu_2\kappa_1)/\mu_1},$$

$$e_7=1+(a+b)(1-k)-(\mu_2\kappa_1)/(\mu_1\kappa_2)$$
$$-\frac{(k+1)(a+b)^2(1-k)}{1+(a+b)(k+1)+(\mu_2\kappa_1)/\mu_1},$$

and δ_{ij} is the Kronecker delta.

The expressions of complex potentials $\Phi_1(z)$ and $\Omega_1(z)$ can be determined from Eqs. (6), (11), (24) and (25).

$$\Phi_1(z)=\frac{\gamma_1}{z-z_0}+c_0+\sum_{k=1}^{+\infty}c_kz^k\quad |z|<R \tag{29}$$

$$\Omega_1(z)=-\frac{\gamma_1}{z-z^*}+\frac{\overline{\gamma_1}z^*(z_0-z^*)}{\bar{z}_0(z-z^*)^2}+d_0+\sum_{k=1}^{+\infty}d_{-k}z^{-k}\quad |z|>R \tag{30}$$

From Eq. (14), the complex potentials $\Phi_2(z)$ and $\Omega_2(z)$ can be derived. Taking the complex conjugate of Eqs. (9) and (10) and rearranging, it is seen that

$$\Psi_1(z)=\frac{R^2}{z^2}\left[\Phi_1(z)+\overline{\Omega_1}\left(\frac{R^2}{z}\right)-z\Phi_1'(z)\right]\quad |z|<R \tag{31}$$

$$\Psi_2(z)=\frac{R^2}{z^2}\left[\Phi_2(z)+\overline{\Omega_2}\left(\frac{R^2}{z}\right)-z\Phi_2'(z)\right]\quad |z|>R \tag{32}$$

The complex potentials $\Psi_1(z)$ and $\Psi_2(z)$ can be calculated using Eqs. (31) and (32), respectively.

Referring to the work of Muskhelishvili (1975), the stress components in the Cartesian coordinates are related to the complex potentials through

$$\sigma_{xx}=\mathrm{Re}[2\Phi(z)-\bar{z}\Phi'(z)-\Psi(z)] \tag{33}$$

$$\sigma_{yy}=\mathrm{Re}[2\Phi(z)+\bar{z}\Phi'(z)+\Psi(z)] \tag{34}$$

$$\sigma_{xy}=\mathrm{Im}[\bar{z}\Phi'(z)+\Psi(z)] \tag{35}$$

In view of Eqs. (33)–(35) and the obtained complex potentials $\Phi_1(z)$, $\Psi_1(z)$, $\Phi_2(z)$ and $\Psi_2(z)$, the stress fields in the inclusion and the matrix regions can be easily derived. Here we omit details for saving space.

4. Image force on edge dislocation

The image force acting on the edge dislocation can be calculated through the Peach–Koehler formula (Hirth and Lothe, 1982)

$$f_x-if_y=\left[\sigma^*_{xy1}(z_0)b_x+\sigma^*_{yy1}(z_0)b_y\right]+i\left[\sigma^*_{xx1}(z_0)b_x+\sigma^*_{xy1}(z_0)b_y\right] \tag{36}$$

where f_x and f_y are the components of the image force in the x- and y-directions, respectively. $\sigma^*_{xx1}(z_0)$, $\sigma^*_{yy1}(z_0)$ and $\sigma^*_{xy1}(z_0)$ are stress components at the dislocation point z_0 (dislocation inside the inclusion), which can be evaluated by the complex potentials $\Phi_{10}(z_0)$ and $\Psi_{10}(z_0)$ in the inclusion.

With the help of Eqs. (33)–(35), the Peach–Koehler formula can be rewritten as (Stagni, 1993)

$$f_x-if_y=\frac{\mu_1(b_y^2+b_x^2)}{\pi(1+\kappa_1)}\left[\frac{\Phi_{10}(z_0)+\overline{\Phi_{10}(z_0)}}{\gamma_1}+\frac{\bar{z}_0\Phi'_{10}(z_0)+\Psi_{10}(z_0)}{\overline{\gamma_1}}\right] \tag{37}$$

Considering Eqs. (6) and (7), the complex potentials $\Phi_{10}(z_0)$, $\Phi'_{10}(z_0)$ and $\Psi_{10}(z_0)$ may be calculated as follows:

$$\Phi_{10}(z_0)=\lim_{z\to z_0}[\Phi_1(z)-\Phi_0(z)] \tag{38}$$

$$\Phi'_{10}(z_0)=\lim_{z\to z_0}\frac{d[\Phi_1(z)-\Phi_0(z)]}{dz} \tag{39}$$

$$\Psi_{10}(z_0)=\lim_{z\to z_0}[\Psi_1(z)-\Psi_0(z)] \tag{40}$$

where $\Phi_0(z)=\frac{\gamma_1}{z-z_0}$ and $\Psi_0(z)=\frac{\overline{\gamma_1}}{z-z_0}+\frac{\gamma_1\bar{z}_0}{(z-z_0)^2}$.

In order to obtain the detailed expression of the complex potential $\Psi_1(z)$, the substitution of Eqs. (29) and (30) into Eq. (31) yields

$$\Psi_1(z)=\frac{R^2}{z^2}\left[\frac{\gamma_1}{z-z_0}+\sum_{k=0}^{+\infty}c_kz^k+\frac{\gamma_1 z}{(z-z_0)^2}-\sum_{k=0}^{+\infty}kc_kz^k+\sum_{k=0}^{+\infty}\overline{d_{-k}}\left(\frac{R^2}{z}\right)^{-k}\right.$$
$$\left.+\frac{\overline{\gamma_1}zz_0}{R^2(z-z_0)}+\frac{\gamma_1(z_0\overline{z_0}-R^2)z^2}{R^2z_0(z-z_0)^2}\right] \tag{41}$$

From Eqs. (38)–(40), the complex potentials $\Phi_{10}(z_0)$, $\Phi'_{10}(z_0)$ and $\Psi_{10}(z_0)$ in the inclusion region can be obtained.

$$\Phi_{10}(z_0)=c_0+\sum_{k=1}^{+\infty}c_kz_0^k \tag{42}$$

$$\Phi'_{10}(z_0)=\sum_{k=1}^{+\infty}kc_kz_0^{k-1} \tag{43}$$

$$\Psi_{10}(z_0)=\frac{R^2}{z_0^2}\left[\sum_{k=0}^{+\infty}c_kz_0^k-\sum_{k=1}^{+\infty}kc_kz_0^k+\sum_{k=0}^{+\infty}\overline{d_{-k}}\left(\frac{R^2}{z_0}\right)^{-k}+\frac{\overline{\gamma_1}z_0}{R^2}+\frac{\gamma_1(z_0\overline{z_0}-R^2)}{R^2z_0}\right]$$
$$-\frac{2\overline{\gamma_2}}{z_0}-\frac{\gamma_2\bar{z}_0}{z_0^2} \tag{44}$$

The expression of the components of the image force f_x and f_y can be found by Eq. (37) together with Eqs. (42)–(44).

If we take $\mu_2=0$ and $\kappa_2=0$, the associated solution of the image force for the case of an edge dislocation inside a nanoscale cylinder with surface stresses can be obtained

If the interface stress vanishes, i.e., $\mu^0=\lambda^0=0$, and the edge dislocation with the Burgers vector $(b_x,0)$ is located at the point $x_0(x_0<R)$ on the x-axis, the image force is reduced to Eq. (15) in the paper of Dundurs and Sendeckyj (1965). Here we omit details for saving space.

The components of the image force along the Burgers vector direction (glide force) and the component perpendicular to the Burgers vector (climb force) are given by (Stagni, 1993)

$$f_g = f_x \cos\theta + f_y \sin\theta \tag{45}$$
$$f_c = f_x \sin\theta - f_y \cos\theta \tag{46}$$

where $\theta = \arctan(b_y/b_x)$.

5. Condition of dislocation stability in inclusion

Consider that a straight-line edge dislocation with Burgers vector b_r (along dislocation glide direction) is assumed to be located inside the inclusion at arbitrary point $z_0 = r_0 e^{i\theta}$ and parallel to the axis of cylindrical nanoscale inclusion. From the above analysis (Sections 2–4), the image force f_r acting on the edge dislocation along the Burgers vector direction (dislocation glide direction) can be derived from the obtained stress fields, which is given by

$$f_r = \frac{\mu_1 b_r^2}{\pi(1+\kappa_1)}\left[\frac{r_0\Phi'_{10}(r_0) + \Psi_{10}(r_0)}{\overline{\gamma_1}}\right] \tag{47}$$

where

$$\Phi'_{10}(z_0) = \sum_{k=1}^{+\infty} k c_k r_0^{k-1}$$

$$\Psi_{10}(r_0) = \frac{R^2}{r_0^2}\left[\sum_{k=0}^{+\infty} c_k r_0^k - \sum_{k=1}^{+\infty} k c_k r_0^k + \sum_{k=0}^{+\infty} \overline{d_{-k}}\left(\frac{R^2}{r_0}\right)^{-k} + \frac{\overline{\gamma_1} r_0}{R^2} + \frac{\gamma_1(r_0^2 - R^2)}{R^2 r_0}\right] - \frac{2\overline{\gamma_2}}{r_0} - \frac{\gamma_2}{r_0}$$

with $\gamma_1 = \frac{-i\mu_1 b_r}{\pi(1+\kappa_2)}$ and $\gamma_2 = \frac{-i\mu_2 b_r}{\pi(1+\kappa_2)}$.

To analyze the stability of the dislocation in the inclusion, the obtained force f_r should be compared with the friction force acting on an edge dislocation in the crystal lattice. As a role, the Peierls stress σ_f gives a dominant contribution in dislocation friction processes (Gryaznov et al., 1991). According to the work of Gryaznov et al. (1991), two parameters are introduced to characterize the dislocation stability in the nanoscale inclusion. The first one, $\Gamma = V_e/V$, is the relative volume of edge dislocation stability, where V is the volume of the inclusion and V_e is the volume of the region of the edge dislocation stability in the inclusion. The second parameter is the critical radius of the cylindrical inclusion R_0 satisfying condition $\Gamma = 1/2$. A comparison of the force f_r and with the friction force gives the condition of edge dislocation stability in the nanoscale inclusion. Here let us introduce the parameter Δf denoting the difference between the image force f_r and the friction force (lattice resistance to the dislocation motion) acting on the edge dislocation

$$\Delta f = |f_r(z_0)| - b_r\sigma_f. \tag{48}$$

In the above equation, if the value of Δf is negative ($\Delta f < 0$), the edge dislocation is stable in the inclusion because the driving force acting on the dislocation is smaller than the friction force. If the value of Δf is positive ($\Delta f > 0$), the edge dislocation is unstable in the inclusion. When we take $\Delta f = 0$, the radius of the cylindrical inclusion R is equal to the critical radius R_0 (Gryaznov et al., 1991).

From the condition in Eq. (48), we can study the critical radius of the cylindrical inclusion R_0 of the edge dislocation stability in the nanoscale inclusion as well as the influence of the interface stress and elastic mismatch on the critical radius. According to the character of the image force f_r acting on the edge dislocation located inside the inclusion and the condition in Eq. (48), the edge dislocation is stable in the inclusion when the following equation is satisfied:

$$\Delta f = \frac{\mu_1 b_r^2}{\pi R(1+\kappa_1)}(\Pi_1 + \Pi_2) - b_r\sigma_f < 0 \tag{49}$$

with

$$\Pi_1 = \frac{1}{\Gamma}(\Pi_3 - \Pi_2) - \frac{C_0}{\Gamma} - \frac{1}{\sqrt{\Gamma}} + \frac{1}{e_5}\left(1 + \frac{1}{\kappa_2}\right)\frac{\mu_2(1+\kappa_1)}{\mu_1(1+\kappa_2)}\frac{1}{\sqrt{\Gamma}} + \sum_{k=1}^{+\infty}\left\{\frac{e_6}{e_5}[(1+k)(\Gamma-1)\Gamma^{k-1.5} - \Gamma^{k-0.5}]\right\} + \sum_{k=1}^{+\infty}\left[\frac{e_7}{e_5}\Gamma^{k-1.5}\right]$$

$$\Pi_2 = \sum_{k=1}^{+\infty}\left\{\frac{e_2}{e_1}k[(1+k)(\Gamma-1)\Gamma^{k-0.5} - \Gamma^{k+0.5}]\right\} - \sum_{k=1}^{+\infty}\left[\frac{e_3}{e_1}k\Gamma^{k-0.5}\right] + \frac{e_4}{e_1}\frac{\mu_2(1+\kappa_1)}{\mu_1(1+\kappa_2)}\sqrt{\Gamma}$$

$$\Pi_3 = C_0 + \sum_{k=1}^{+\infty}\left\{\frac{e_2}{e_1}[(1+k)(\Gamma-1)\Gamma^{k-0.5} - \Gamma^{k+0.5}]\right\} - \sum_{k=1}^{+\infty}\left[\frac{e_3}{e_1}\Gamma^{k-0.5}\right] + \frac{e_4}{e_1}\frac{\mu_2(1+\kappa_1)}{\mu_1(1+\kappa_2)}\sqrt{\Gamma}$$

$$C_0 = \frac{1}{1+e}\left[\frac{a+2b}{1+b+(\mu_2\kappa_1)/\mu_1}\frac{1}{\sqrt{\Gamma}} + \frac{a}{1+b+(\mu_2\kappa_1)/\mu_1}\sqrt{\Gamma}\right]$$

where parameter Γ should be satisfied the condition of the dislocation stability ($\Gamma = 1/2$ in Gryaznov et al., 1991) for studying the critical value of the radius of the inclusion.

6. Numerical examples and discussion

In this section, numerical examples are given to discuss the image force acting on the edge dislocation and the equilibrium position of the dislocation inside the inclusion through Eqs. (45) and (46). Additionally, the critical radius of the cylindrical inclusion R_0 for edge dislocation stability in the inclusion and the influence of the interface stress and elastic mismatch on it can be investigated through Eq. (49). In subsequent numerical calculation, we define the relative shear modulus $\varepsilon = \mu_2/\mu_1$ and the intrinsic lengths $\alpha = \mu^0/\mu_1$ and $\beta = \lambda^0/\mu_1$ (Lim et al., 2006). According to the results in Miller and Shenoy (2000), the absolute values of the intrinsic lengths α and β are about 0.1 nm.

6.1. Analysis of image force on edge dislocation

From Eqs. (45) and (46), the influence of the material elastic dissimilarity and interface stress as well as Burgers vector direction upon the glide/climb force acting on the edge dislocation can be evaluated in detail when a single edge dislocation is located in the inclusion. Here, we will mainly focus on the impact of the interface stress on the glide/climb force. Suppose that the edge dislocation lies at the point x_0 on the x-axis in the inclusion. The relative location of the dislocation is defined as $\rho = x_0/R$ and the normalized glide force and climb force are defined as $f_{go} = \pi R(1+\kappa_1)f_g/[\mu_1(b_x^2 + b_y^2)]$ and $f_{co} = \pi R(1+\kappa_1)f_c/[\mu_1(b_x^2 + b_y^2)]$.

The variation of the normalized glide force f_{go} versus the radius R is depicted in Fig. 2 with different values of the relative shear modulus ε and two different sets of intrinsic lengths α and β for $\nu_1 = \nu_2 = 0.25$, $\rho = 0.9$ and $b_y = 0$. Note that the climb force equals to zero in this case. It can be found that, if interface constants are positive ($\alpha > 0$ and $\beta > 0$), the edge dislocation in the inclusion will be repelled by the interface; if interface constants

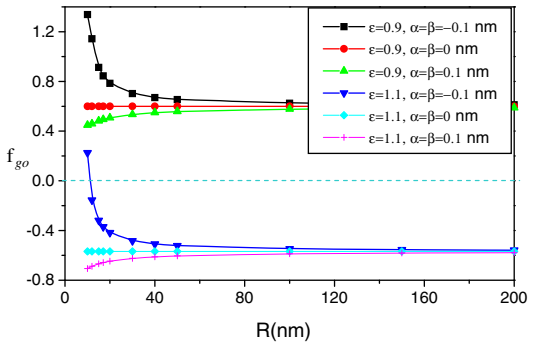

Fig. 2. The normalized glide force f_{go} versus the radius R with different values of the relative shear modulus ε and two different sets of intrinsic lengths α and β for $\nu_1 = \nu_2 = 0.25$, $\rho = 0.9$ and $b_y = 0$.

are negative ($\alpha < 0$ and $\beta < 0$), the edge dislocation will be attracted by the interface. An additional repulsive force or attractive force will act on the edge dislocation along glide direction due to consider the interface effects, which causes the total glide force to increase or decrease. The phenomenon cannot be predicted by the classical elasticity without considering the effect of interface stress ($\alpha = 0$ and $\beta = 0$). This result indicates that the local hardening and softening at the interface can be produced for considering the interface stresses, which is similar to the imperfect soft or stiff interface studied by Benveniste and Miloh (2001).

The additional force (repulsive force or attractive force) increases with the decrease of the inclusion radius, and the size dependence becomes significant when the inclusion radius is very small. An interesting result is that, for the case of $\alpha = -0.1$ nm, $\beta = -0.1$ nm and $\varepsilon = \mu_2/\mu_1 = 1.1$, the direction of the normalized image force may be changed when the radius of the inclusion reduces to a small value (about 10 nm in Fig. 2). The reason of this phenomenon is that the attractive force acting on the edge dislocation produced by the interface ($\alpha = -0.1$ nm and $\beta = -0.1$ nm) will increase with the decrease of the radius of the inclusion and the attractive force will be larger than the repulsive force produced by the stiff matrix ($\varepsilon = \mu_2/\mu_1 = 1.1$) leading to the change of the direction of the image force when the value of the radius is smaller than 10 nm. The effect of interface stress becomes negligible when the radius of the inclusion is relatively large. The classical case (without interface stress) is, as expected, independent of the inclusion size and cannot change the orientation of the glide force.

The variation of the normalized climb force f_{co} versus the radius R is depicted in Fig. 3 with different values of the relative shear modulus ε and two different sets of intrinsic lengths α and β for $\nu_1 = \nu_2 = 0.25$, $\rho = 0.9$ and $b_x = 0$. In this case the glide force equals to zero. The parallel results can be obtained from this figure for climb force. However, the impact of the interface stress on the climb force is clearly larger than that on glide force. The size dependence becomes important if the inclusion radius is below a small value (about 60 nm in Fig. 3). The climb force will change the original direction, when the radius of the inclusion equals to 20 nm, for certain intrinsic lengths and the ratio of the shear moduli of two bulk solids.

The normalized glide force f_{go} as a function of the relative location ρ with different values of ε is plotted in Fig. 4 for $\alpha = -0.1$ nm and $\beta = -0.1$ nm ($\nu_1 = \nu_2 = 0.25$, $R = 10$ nm and $b_y = 0$). It is seen from Fig. 4 that, when the edge dislocation approaches the interface from the origin, the stiff matrix ($\varepsilon = \mu_2/\mu_1 = 1.1$) first repels the edge dislocation and then attracts it due to consider negative interface stress. There is an unstable equilibrium position on the x-axis and the glide force equals to zero at that point. To our knowledge, the stiff matrix will always repel the edge dislocation located within the inclusion in the classical elasticity (the associated plot has been given in Fig. 4). The soft matrix and the negative interface stress always attract the edge dislocation when it is near to the interface.

The normalized climb force f_{co} as a function of the relative location ρ with different values of ε is plotted in Fig. 5 for $\alpha = 0.1$ nm and $\beta = 0.1$ nm ($\nu_1 = \nu_2 = 0.25$, $R = 10$ nm and $b_x = 0$). It is found from Fig. 5 that the soft matrix ($\varepsilon = \mu_2/\mu_1 = 0.9$) and the positive interface stress first attracts then repels the edge dislocation inside the inclusion. There is a stable equilibrium position on the x-axis and the climb force equals to zero at that point. The hard matrix and the positive interface stress always repel the edge

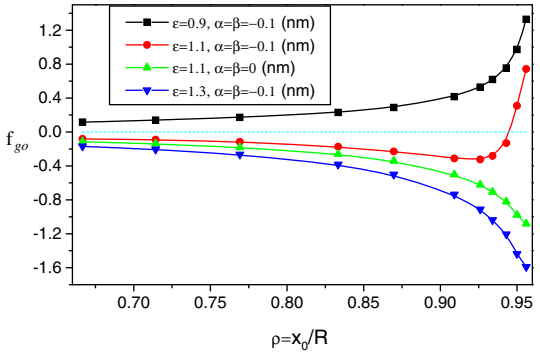

Fig. 4. The normalized glide force f_{go} as a function of the relative location ρ with different values of ε for $\alpha = -0.1$ nm and $\beta = -0.1$ nm ($\nu_1 = \nu_2 = 0.25$, $R = 10$ nm and $b_y = 0$).

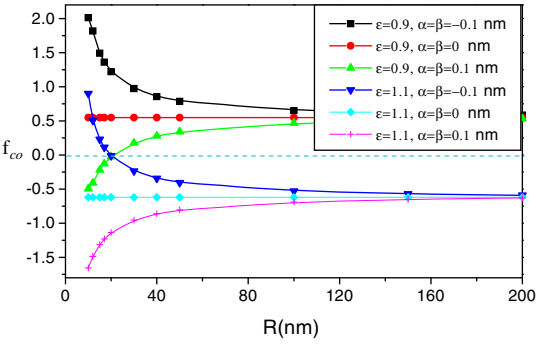

Fig. 3. The normalized climb force f_{co} versus the radius R with different values of the relative shear modulus ε and two different sets of intrinsic lengths α and β for $\nu_1 = \nu_2 = 0.25$, $\rho = 0.9$ and $b_x = 0$.

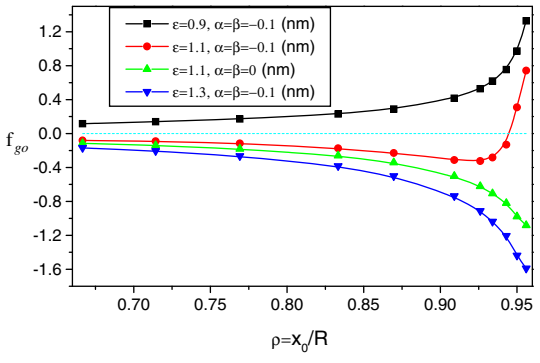

Fig. 5. The normalized climb force f_{co} as a function of the relative location ρ with different values of ε for $\alpha = -0.1$ nm and $\beta = -0.1$ nm ($\nu_1 = \nu_2 = 0.25$, $R = 10$ nm and $b_x = 0$).

dislocation inside the inclusion. The results from Figs. 4 and 5 show that there is a significant local softening or hardening at the interface of the nanoscale inclusion. Comparing with the classical solution, the mobility of the edge dislocation in the nanoscale inclusion with interface stress becomes more complex under the same conditions.

The glide force f_{go} as a function of α with different values of R is shown in Fig. 6 for $\rho = 0.9$, $\varepsilon = 1.1$, $\beta = -0.1$ nm and $\nu_1 = \nu_2 = 0.25 (b_y = 0)$. It is seen that the larger the absolute value of intrinsic lengths α, the larger effect of the interface stress upon the glide force. At the same time, the smaller radius of the inclusion, the larger effect of the interface stress. On the contrary, the interface effect becomes negligible when the radius of the inclusion is relatively large. The glide force f_{go} as a function of β with different values of R is shown in Fig. 7 for $\rho = 0.9$, $\varepsilon = 1.1$, $\alpha = -0.1$ nm and $\nu_1 = \nu_2 = 0.25$ ($b_y = 0$). Conclusions parallel to the results in Fig. 6 can be derived.

Figs. 8 and 9 illustrate the variation of the glide force f_{go} and the climb force f_{co} versus the direction of the Burgers vector for $\rho = 0.9$, $\varepsilon = 1.1$, $\nu_1 = \nu_2 = 0.25$ and $R = 10$ nm. It is seen that the glide force f_{go} is always negative for classical solution. However, if the negative interface constants are considered, the glide force is negative first, and then becomes positive with the increment of the angle θ (the direction of the Burgers vector relative to the x-axis). The special case is that the glide force along the direction of the Burgers vector equals to zero around $\theta = 48^\circ$ which differs from the classical solution. The absolute value of the glide force for considering positive interface constants is always larger than that for classical solution. The effect of the interface stress on the glide force is largest around $\theta = 48^\circ$. It is found from Fig. 9 that the climb force f_{co} is also negative for classical solution. It will be negative first, and then becomes positive with the increment of the angle θ if the negative interface effect is added. Similarly, the climb force perpendicular to the direction of the Burgers vector equals to zero around $\theta = 65^\circ$. The effect of the interface stress on the climb force is largest for $\theta = 90^\circ$. The results show that, when the direction of the Burgers vector of the edge dislocation is various, the influence of the interface stress on the glide force and climb force is significant.

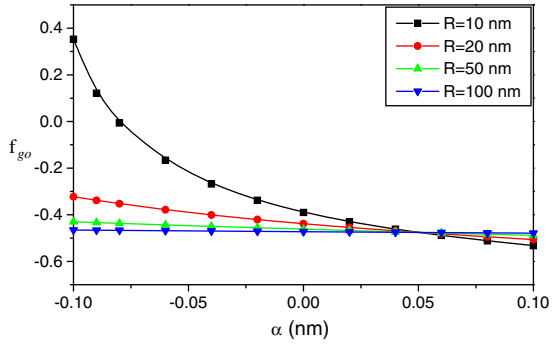

Fig. 6. The normalized glide force f_{go} as a function of the intrinsic length α with different values of R for $\rho = 0.9$, $\varepsilon = 1.1$, $\beta = -0.1$ nm and $\nu_1 = \nu_2 = 0.25$ ($b_y = 0$).

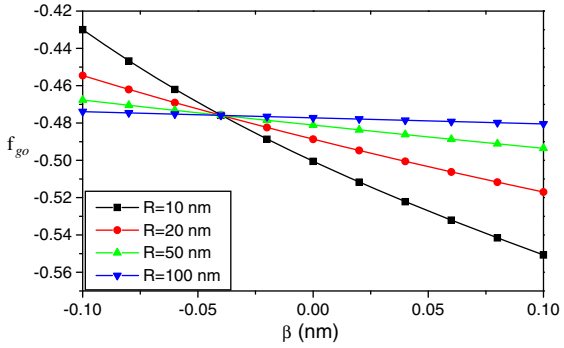

Fig. 7. The normalized glide force f_{go} as a function of the intrinsic length β with different values of R for $\rho = 0.9$, $\varepsilon = 1.1$, $\alpha = -0.1$ nm and $\nu_1 = \nu_2 = 0.25$ ($b_y = 0$).

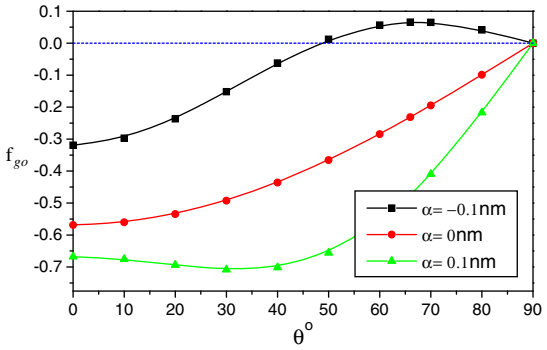

Fig. 8. The normalized glide force f_{go} as a function of the direction of the Burgers vector θ with different values of α for $\rho = 0.9$, $\varepsilon = 1.1$, $\nu_1 = \nu_2 = 0.25$, $\beta = 0$ and $R = 10$ nm.

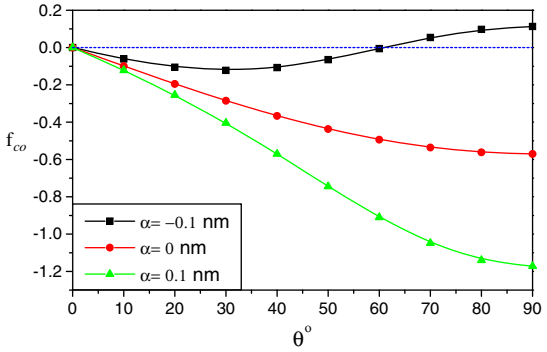

Fig. 9. The normalized climb force f_{co} as a function of the direction of the Burgers vector θ with different values of α for $\rho = 0.9$, $\varepsilon = 1.1$, $\nu_1 = \nu_2 = 0.25$, $\beta = 0$ and $R = 10$ nm.

6.2. Analysis of dislocation stability

Here, we utilize Eq. (49) to study the edge dislocation stability in the inclusion and the influence of the interface stress and elastic mismatch on it. In subsequent numerical calculation, we define $\Delta f_0 = \Delta f/(b_r \sigma_f)$. The material constants of the inclusion is taken

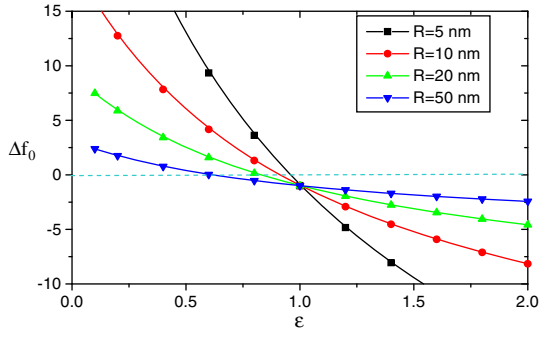

Fig. 10. The value of Δf_0 as a function of the relative shear modulus $\varepsilon = \mu_2/\mu_1$ with different values of the radius of the inclusion R for $\alpha = \beta = 0$ and $\nu_1 = \nu_2 = 0.34$.

from Gryaznov and Trusov (1993) ($\mu_1 = 33$ GPa, $\nu_1 = 0.34$, $b_r = 0.256$ nm and $\sigma_f = 1.67 \times 10^{-2}$ GPa).

The value of Δf_0 is plotted as a function of the relative shear modulus $\varepsilon = \mu_2/\mu_1$ in Fig. 10 with different values of the radius of the inclusion for $\alpha = \beta = 0$ and $\nu_1 = \nu_2 = 0.34$. In this case, it can be seen that, if $\varepsilon \geqslant 1$ (the shear modulus of the matrix is larger than that of the inclusion), the edge dislocations in the inclusion are absolutely stable ($\Delta f_0 < 0$). The relative shear modulus ε to keep dislocation stabilization inside the inclusion will decrease with the increment of the radius of inclusion. The result also shows that, if the radius of the inclusion is changeless, there is a critical value of the relative shear modulus ε to change the edge dislocation stability in the inclusion. If the value of ε is larger than the critical value, the edge dislocation is stable in the inclusion.

The value of Δf_0 is plotted as a function of ν_2 in Fig. 11 with different values of the radius of the inclusion for $\alpha = \beta = 0$, $\nu_1 = 0.34$ and $\varepsilon = \mu_2/\mu_1 = 1$. It is found that, if the radius of the inclusion is changeless, there also exists a critical value of ν_2 to alter the edge dislocation stability in the inclusion. When the value of ν_2 is less than the critical value, the edge dislocation is unstable in the inclusion.

The variation of the value of Δf_0 with respect to the relative shear modulus $\varepsilon = \mu_2/\mu_1$ is depicted in Fig. 12 with different values of intrinsic lengths α and β for $R = 6$ nm and $\nu_1 = \nu_2 = 0.34$. It is seen that, if $\alpha = \beta = 0$ (the interface stress vanishes) and $\alpha = \beta = 0.15$ nm, the edge dislocations in the inclusion are stable for $\varepsilon = 1$. However, if we take $\alpha = \beta = -0.15$ nm, the edge dislocations in the inclusion are unstable ($\Delta f_0 > 0$) for $\varepsilon = 1$. The phenomenon cannot be predicted by the classical elasticity solution ($\alpha = \beta = 0$) without considering the effect of interface stress. Fig. 12 also shows that, if the positive interface stress is considered, the critical value of the relative shear modulus to keep the dislocation stabilization in the inclusion will decrease; if the negative interface stress is considered, it will increase. These results indicate that, when the radius of the inclusion is fixed, the effect of the interface stress on the critical value of the relative shear modulus is significant.

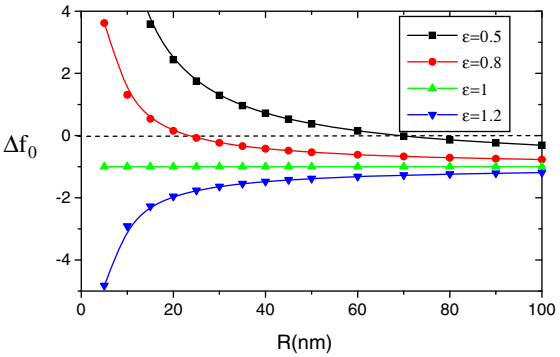

Fig. 13. The value of Δf_0 a function of the radius of inclusion R with different values of the relative shear modulus ε for $\alpha = \beta = 0$ and $\nu_1 = \nu_2 = 0.34$.

If we take $\alpha = \beta = 0$, the value of Δf_0 is plotted as a function of the radius of inclusion R in Fig. 13 with different values of the relative shear modulus $\varepsilon(\nu_1 = \nu_2 = 0.34)$ and in Fig. 14 with different values of $\nu_2(\varepsilon = 1)$. It can be found from two Fig. that, if $\varepsilon < 1$ (the shear modulus of the matrix is less than that of the inclusion) or $\nu_2 < \nu_1$ (the Poisson's ratio of the matrix is less than that of the inclusion), there always exists a critical value of the radius of the inclusion to alter the edge dislocations stability in the inclusion. If the radius of the inclusion is larger than the critical value, the edge dislocations are stable in the inclusion. When the value of

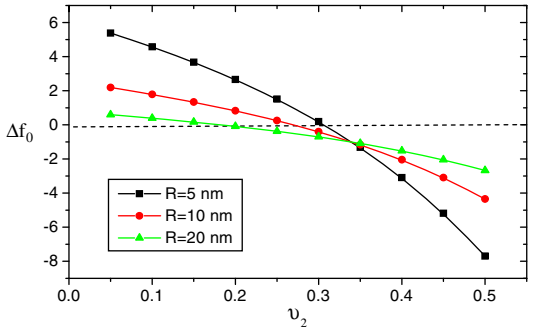

Fig. 11. The value of Δf_0 as a function of the Poisson's ratio of the matrix ν_2 with different values of the radius of the inclusion R for $\alpha = \beta = 0$, $\nu_1 = 0.34$ and $\varepsilon = 1$.

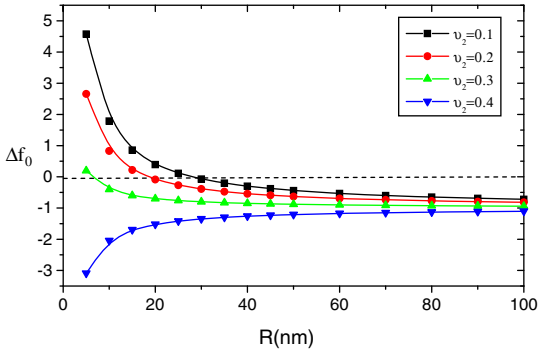

Fig. 14. The value of Δf_0 as a function of the radius R with different values of the Poisson's ratio of the matrix ν_2 for $\alpha = \beta = 0$ and $\varepsilon = 1$.

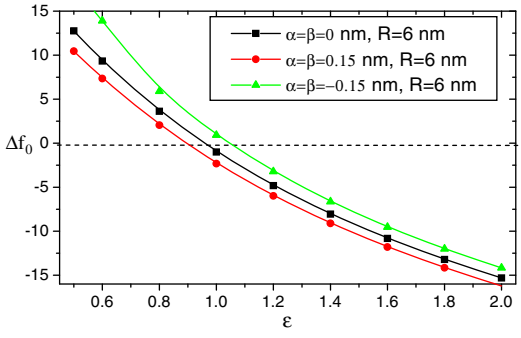

Fig. 12. The value of Δf_0 with respect to the relative shear modulus $\varepsilon = \mu_2/\mu_1$ with different values of intrinsic lengths α and β for $R = 6$ nm and $\nu_1 = \nu_2 = 0.34$.

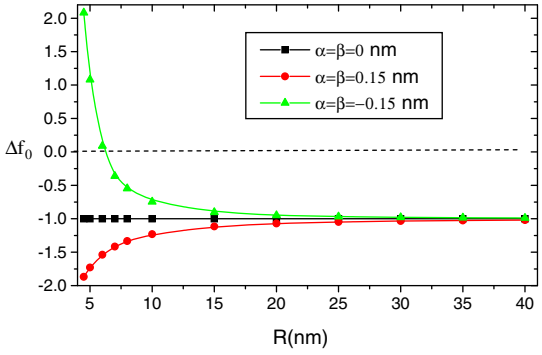

Fig. 15. The value of Δf_0 as a function of the radius R with different values of intrinsic lengths α and β for $\varepsilon = 1$ and $\nu_1 = \nu_2 = 0.34$.

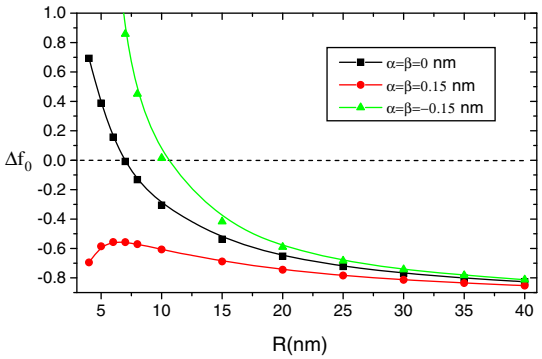

Fig. 16. The value of Δf_0 as a function of the radius R with different values of intrinsic lengths α and β for $\varepsilon = 0.8$ and $\nu_1 = \nu_2 = 0.34$.

the shear modulus (or the Poisson's ratio) of the inclusion is changeless, the critical value of the radius of the inclusion will increase with the decrease of the shear modulus or the Poisson's ratio of the matrix.

The variation of the value of Δf_0 as a function of the radius R with different values of intrinsic lengths α and β is depicted in Fig. 15 for $\varepsilon = 1$ and in Fig. 16 for $\varepsilon = 0.8$. It is found from Fig. 15 that, if $\alpha = \beta = 0$ (the interface stress vanishes) or $\alpha = \beta = 0.15$ nm, the edge dislocations in the inclusion are absolutely stable. An interesting result is that, if $\alpha = \beta = -0.15$ nm and $\varepsilon = 1$, the edge dislocations in the inclusion are unstable when the radius of inclusion is taken a very small value. Fig. 15 shows that, the positive interface stress can consolidate the edge dislocation stability in the inclusion and the negative interface stress can destroy the dislocation stability. It is seen from Fig. 16 that, if $\alpha = \beta = 0$ and $\alpha = \beta = -0.15$ nm, the edge dislocations in the inclusion are unstable when the radius of inclusion is very small. The critical radius of the dislocation stability in the nanoscale inclusion for $\alpha = \beta = -0.15$ nm is larger than that for $\alpha = \beta = 0$. However, the edge dislocations are always stable for $\alpha = \beta = 0.15$ nm which differs from the classical elasticity solution ($\alpha = \beta = 0$). The results show that the interface stress can change not only the property of the edge dislocation stability in the nanoscale inclusion, but also the value of the critical radius of the inclusion under certain conditions.

7. Conclusions

The problem of an edge dislocation located within a circular nanoscale cylindrical inclusion in an unbounded matrix is first studied by using the interface stress model. The explicit solutions of stress fields and the image force on the edge dislocation are given explicitly by using the complex variable method. The influence of the interface stress on the image force acting on the edge dislocation is evaluated in detail. In addition, the stability of straight-line edge dislocations inside a nanoscale inclusion is also investigated theoretically. Some conclusions drawn from Section 6 are summarized as:

(1) An additional repulsive force or attractive force acting on the edge dislocation (inside the inclusion) can be produced due to consider the interface stress, which causes the total glide/climb force to increase or decrease. This additional force will increase with the decrease of the inclusion radius, and the original direction of the glide/climb force may be changed when the radius of the inclusion reduces to a small value.

(2) When the shear modulus of the inclusion is less than that of the matrix (the Poisson's ratio $\nu_1 = \nu_2$), there is an unstable equilibrium position of the edge dislocation inside the inclusion if the negative interface stress is considered; and no equilibrium position is available if the positive interface stress is considered. When the shear modulus of the inclusion is larger than that of the matrix (the Poisson's ratio $\nu_1 = \nu_2$), there is a stable equilibrium position of the edge dislocation inside the inclusion if the positive interface stress is considered; and no equilibrium position is available if the negative interface stress is considered.

(3) When the direction of the Burgers vector of the edge dislocation is various, the influence of the interface stress on the glide force and climb force is significant. Comparing with the classical solution, the mobility of the edge dislocation in the nanoscale inclusion with interface stress becomes more complex under the same external conditions.

(4) If the material constants of the inclusion are fixed, a critical value of the shear modulus or the Poisson's ratio of the matrix may exist to change the edge dislocation stability in the inclusion. When the value of the shear modulus or the Poisson's ratio of the matrix is larger than the critical value, the dislocation is stable in the inclusion. On the other hand, if the positive interface stress is considered, the critical value to keep the dislocation stabilization in the inclusion will decrease; if the negative interface stress is considered, it will increase.

(5) When the shear modulus of the matrix is less than that of the inclusion or $\nu_2 < \nu_1$ (the Poisson's ratio of the matrix is less than that of the inclusion), there always exists a critical value of the radius of the inclusion to alter the edge dislocations stability in the inclusion. If the value of the radius of the inclusion is larger than the critical value, the dislocation is stable in the inclusion. The critical radius of the inclusion increases with the decrease of the shear modulus or the Poisson's ratio of the matrix. In addition, the critical radius will increase for considering the negative interface stress and will decrease for considering the positive interface stress.

Acknowledgments

The authors would like to deeply appreciate the support by the National Natural Science Foundation of China (50801025 and 10872065), China Postdoctoral Science Foundation and Aid program for Science and Technology Innovative Research Team in Higher Educational Institutions of Hunan Province.

References

Benveniste, Y., Miloh, T., 2001. Imperfect soft and stiff interfaces in two-dimensional elasticity. Mechanics of Materials 33 (6), 309–323.
Chen, Q., Biner, S.B., 2005. Stability of perfect dislocations in rare-earth intermetallic compounds: YCu YAg and YZn. Acta Materialia 53, 3215–3223.
Chen, T., Dvorak, G.J., 2006. Fibrous nanocomposites with interface stress: Hill's and Levin's connections for effective moduli. Applied Physics Letters 88, 211912–211915.
Chen, T., Dvorak, G.J., Yu, C.C., 2007. Solids containing spherical nano-inclusions with interface stresses: effective properties and thermal–mechanical connections. International Journal of Solids and Structures 44, 941–955.
Duan, H.L., Karihaloo, B.L., 2007. Thermo-elastic properties of heterogeneous materials with imperfect interfaces: generalized Levin's formula and Hill's connections. Journal of the Mechanics and Physics of Solids 55, 1036–1052.
Duan, H.L., Wang, J., Huang, Z.P., Karihaloo, B.L., 2005. Size-dependent effective elastic constants of solids containing nano-inhomogeneities with interface stress. Journal of the Mechanics and Physics of Solids 53, 1574–1596.
Dundurs, J., Mura, T., 1964. Interaction between an edge dislocation and a circular inclusion. Journal of the Mechanics and Physics of Solids 12, 177–189.
Dundurs, J., Sendeckyj, G.P., 1965. Edge dislocation inside a circular inclusion. Journal of the Mechanics and Physics of Solids 13, 141–147.
Fang, Q.H., Liu, Y.W., 2006. Size-dependent interaction between an edge dislocation and a nanoscale inhomogeneity with interface effects. Acta Materialia 54, 4213–4220.

Gryaznov, V.G., Trusov, L.I., 1993. Size effects in micromechanics of nanocrystals. Progress in Materials Science 37, 289–401.
Gryaznov, V.G., Kaprelov, A.M., Romanov, A.E., 1989. Size effect of dislocation stability in small particles and microcrystallites. Scripta Materialia 23, 1443–1448.
Gryaznov, V.G., Polonsky, I.A., Romanov, A.E., Trusov, L.I., 1991. Size effects of dislocation stability in nanocrystals. Physical Review B 44, 42–46.
Gurtin, M.E., Murdoch, A.I., 1975. A continuum theory of elastic material surfaces. Archive of Rational Mechanics and Analysis 57, 291–323.
Gurtin, M.E., Weissmuller, J., Larche, F., 1998. A general theory of curved deformable interfaces in solids at equilibrium. Philosophical Magazine A 78, 1093–1109.
Hirth, J.P., Lothe, J., 1982. Theory of Dislocations, second ed. Wiley, New York.
Lim, C.W., Li, Z.R., He, L.H., 2006. Size dependent, non-uniform elastic field inside a nano-scale spherical inclusion due to interface stress. International Journal of Solids and Structures 43, 5055–5065.
Liu, Y.W., Fang, Q.H., Jiang, C.P., 2004. A piezoelectric screw dislocation interacting with an interphase layer between a circular inclusion and the matrix. International Journal of Solids and Structures 41, 3255–3274.
Luo, H.A., Chen, Y., 1991. An edge dislocation in a three-phase composites cylinder. Journal of Applied Mechanics 58, 75–86.
Ma, C.C., Lu, H.T., 2006. Theoretical analysis of screw dislocations and image forces in anisotropic multilayered media. Physical Reviews B 73, 144102.
Miller, R.E., Shenoy, V.B., 2000. Size-dependent elastic properties of nanosize Structural elements. Nanotechnology 11, 139–147.
Muskhelishvili, N.L., 1975. Some Basic Problems of Mathematical Theory of Elasticity. Noordhoff, Leyden.
Nembach, E., 1996. Particle Strengthening of Metals and Alloys. Wiley, New York.
Qaissaunee, M.T., Santare, M.H., 1995. Edge dislocation interaction with an elliptical inclusion surrounding by an interfacial zone. Quarterly Journal of Mechanics and Applied Mathematics 48, 465–482.
Quang, H.Le., He, Q.C., 2007. Size-dependent effective thermoelastic properties of nanocomposites with spherically anisotropic phases. Journal of the Mechanics and Physics of Solids 55, 1899–1931.
Romanov, A.E., 1995. Continuum theory of defects in nanoscaled materials. Nanostructured Materials 6, 125–134.
Schoeck, G., 1997. Stability of dislocation arrays. Scripta Materialia 37, 1407–1408.
Sharma, P., Ganti, S., 2004. Size-dependent Eshelby's tensor for embedded nano-inclusions incorporating surface/interface energies. Journal of Applied Mechanics 71, 663–671.
Sharma, P., Ganti, S., Bhate, N., 2003. Effect of surfaces on the size-dependent elastic state of nano-inhomogeneities. Applied Physics Letters 82, 535–537.
Stagni, L., 1993. Edge dislocation near an elliptic inhomogeneity with either an adhering or a slipping interface: a comparative study. Philosophical Magazine A 68, 49–57.
Stagni, L., 1999. The effect of the interface on the interaction of an interior edge dislocation with an elliptical inhomogeneity. Journal of Applied Mathematical Physics (ZAMP) 50, 327–337.
Takahashi, A., Ghoniem, N.M., 2008. A computational method for dislocation–precipitate interaction. Journal of the Mechanics and Physics of Solids 56, 1534–1553.
Tian, L., Rajapakse, R.K.N.D., 2007. Elastic field of an isotropic matrix with a nanoscale elliptical inhomogeneity. International Journal of Solids and Structures 44, 7988–8005.
Wang, Z., 1998. Experimental study of the thermal stability of dislocation structures produced through cyclic deformation in copper polycrystals. Scripta Materialia 39, 493–500.
Wang, X., Sudak, L.J., 2006. Interaction of a screw dislocation with an arbitrary shaped elastic inhomogeneity. Journal of Applied Mechanics 73, 206–211.
Wang, X., Pan, E., Roy, A.K., 2007. New phenomena concerning a screw dislocation interacting with two imperfect interfaces. Journal of the Mechanics and Physics of Solids 55, 2717–2734.
Warren, W.E., 1983. Edge dislocation inside an elliptical inclusion. Mechanics of Materials 2, 319–330.
Weinberger, C.R., Cai, W., 2007. Computing image stress in an elastic cylinder. Journal of the Mechanics and Physics of Solids 55, 2027–2054.
Xiao, Z.M., Chen, B.J., 2001. On the interaction between an edge dislocation and a coated inclusion. International Journal of Solids and Structures 38, 2533–2548.
Yoo, M.H., Yoshimi, K., Hanada, S., 1999. Dislocation stability and deformation mechanisms of iron aluminides and silicide. Acta Materialia 47, 3579–3588.
Zhang, T.Y., Qian, C.F., 1996. Interaction of a screw dislocation with a thin-film-covered mode III crack. Acta Materialia 44, 4513–4520.